Volume 1 | Number 1 | Jan 2013 | Pages 1–100

Nanoscale

www.rsc.org/nanoscale

ROYAL SOCIETY OF CHEMISTRY

www.rsc.org/nanoscale

Depositing CdS Nanoclusters on Carbon-modified NaYF$_4$:Yb,Tm Upconversion Nanocrystals for NIR-light Enhanced Photocatalysis

Meijie Tou,† Yuanyuan Mei,† Song Bai,* Zhenguo Luo, Yong Zhang and Zhengquan Li*

Institute of Physical Chemistry and Department of Chemistry, Zhejiang Normal University, Jinhua, Zhejiang 321004, P. R. China

E-mail: zqli@zjnu.edu.cn (Z. Li); songbai@zjnu.edu.cn (S.Bai)

† Equal contribution.

Abstract: High-quality hexagonal NaYF$_4$:Yb,Tm upconversion nanocrystals (UCNs) prepared in organic solutions display uniform sizes and strong UC emissions, but they possess a hydrophobic surface which hinder them to combine with various semiconductor nanocrystals (NCs) to form a hybrid NIR-activated photocatalyst. Herein we present a facile approach to modify the hydrophobic UCNs with a uniform carbon layer and enable them with hydrophilicity and surface functionalization. The carbon shell provides a good substrate for enriching metal ions and *in situ* generating CdS nanoclusters on the particle surface which can utilize both the upconverted UV and visible emissions. The developed NaYF$_4$:Yb,Tm@C@CdS nanoparticles were characterized with TEM, SEM, XRD, PL and UV-Vis spectra and their formation mechanism is elucidated. The products display good photocatalytic activity under the visible light and obviously enhanced performance under the Vis-NIR light, due to the efficient utilization of UC emissions and strong adsorption capacity of the carbon shell. The working mechanism of the hybrid photocatalysts is also proposed.

Keywords: hybrid photocatalysts; core-shell nanoparticles; upconversion; CdS.

1. Introduction

Environmental pollution and energy shortage are both global crises and threats to the long-term development of human society.[1-3] Among potential solutions, semiconductor photocatalysis utilizing solar energy for environmental remedy is considered as an economic, renewable, clean and safe technology.[4-6] However, one big limitation of semiconductors photocatalysis is the narrow absorption range of semiconductors which can only make use of the ultraviolet (UV) or visible (Vis) light. Although many strategies have been made to broaden or extent the absorption range of semiconductors such as doping, dye sensitization, and coupling with noble metals or other semiconductors, the main absorption of most semiconductors is still limited in the UV or Vis region.[7-10] Utilization of solar energy in the near-infrared (NIR) region is still rarely explored while the NIR light occupies *ca.* 48% in the solar spectrum.[11-13] To overcome this limitation, creation of hybrid photocatalysts with upconversion nanocrystals (UCNs) as light converter has been regarded as one of the promising solutions.[14-15] With the capability of upconverting NIR photons to be the UV and/or Vis ones, the UCNs can absorb NIR light and activate the semiconductors for photocatalytic applications. Development of uniform and efficient UCN-semiconductor hybrid nanostructures is thus of great importance to achieve such kind of NIR-activated photocatalysts.

In a hybrid NIR-activated photocatalyst, the activate ability for the semiconductor relies on the UC emissions of the UCNs. Thus, the overlap of emission and absorption spectra between the UCNs and the semiconductors is a very important parameter to determine their photocatalytic efficiency. Nowadays, hexagonal-phase (β-) NaYF$_4$:Yb,Tm NCs has been proven to be one of the best UC phosphors and combination of NaYF$_4$:Yb,Tm NCs with TiO$_2$ or ZnO shells has been extensively explored.[16-18] However, it is known that NaYF$_4$:Yb,Tm NCs exhibit strong blue emissions and relatively low UV emissions, while the TiO$_2$ and ZnO shells can only harness the UV emissions. For efficient utilization of the upconverted Vis emissions, combination of NaYF$_4$:Yb,Tm NCs with a narrow band gap semiconductor such as CdS should be a better choice.[19] But different from the synthesis of TiO$_2$ shell which can be achieved *via* traditional sol-gel process, the preparation of uniform core-shell structured UCNs with other semiconductor is still challenging, due to the difference in growing habits and/or conditions for different NCs. Recently, Yu *et al* attempted the

synthesis of a hybrid photocatalyst consisting of $NaYF_4$:Yb,Tm microrods and CdS NCs.[20] The synthesis involved the individual preparation of $NaYF_4$:Yb,Tm and CdS particles, functionalizing them with different groups, and then linking them through molecular chains. Such a process is very tedious and the developed $NaYF_4$:Yb,Tm/CdS photocatalysts exhibit a large particle size, low UC fluorescence, and easy aggregation in solution. Furthermore, the stability of such hybrid particles is also problematic because of the low thermal stability of molecular chains and the high mobility of solid NCs in solution. It is highly desirable to develop convenient and reliable approaches to synthesize hybrid NIR-activated photocatalysts with high uniformity, strong UC emissions, excellent dispersibility, and high structural stability.

In contrast to the UCNs prepared under hydrothermal condition, the UCNs obtained from high-temperature organic solution are more uniform in size and stronger in UC fluorescence.[21-22] However, a big limitation of these high-quality UCNs is their hydrophobic surface, hindering them to be dispersed in aqueous solution. On the other hand, to avoid the tedious process of surface modification and molecular linking of two types of NCs, direct deposition of the semiconductor NCs on the UCNs is preferred. But this synthetic strategy requires a hydrophilic, functional and active surface on the UCNs as a substrate. Carbon spheres composed of carbonous polymer possess a hydrophilic and flexible surface with many functional groups, which are highly suspended in aqueous solution and have been widely used as templates to deposit various oxide and sulfide semiconductor NCs.[23-24] If a carbon shell could be covered on the hydrophobic UCNs, the carbon-coated UCNs will become hydrophilic and build a versatile surface for the hybridization of various semiconductor NCs. Furthermore, carbon shell can efficient absorb and enrich the polluted species round the hybrid photocatalysts, which can also greatly enhance the photocatalytic effect.[25-27] Moreover, some literatures have also suggested that carbon shell can harvest some Vis light and facilitate the electron-hole separation for the photocatalysts.[28-29] These features may also benefit the overall photocatalytic efficiency of the hybrid NIR-activated photocatalysts.

In this work, we present a facile route to formulate hybrid NIR-activated photocatalysts by coating a uniform carbon shell on the hydrophobic UCNs and then directly depositing semiconductor NCs on their surface. As a proof-of-concept work, we employed uniform β-$NaYF_4$:Yb,Tm nanoplates as the UCNs and CdS nanoclusters as the semiconductor NCs. Specifically, we developed a reverse micelle approach to

coat a uniform carbon shell on the $NaYF_4$:Yb,Tm nanoplates though carbonization of glucose. The carbon shell can efficiently enrich the metal ions and serve as a powerful substrate for directly generating CdS NCs on the $NaYF_4$:Yb,Tm nanoplates. The developed core-shell $NaYF_4$:Yb,Tm@C@CdS NPs exhibit strong UC emissions, uniform sizes, and strong capability of adsorbing the polluted species. This hybrid photocatalyst can be directly used for the degradation of various dyes pollutants under Vis light, and exhibit enhanced activity under the Vis-NIR light. This work may shed some new lights on the design and synthesis of hybrid photocatalysts and applying them for environmental applications.

2. Experimental

2.1 Preparation of β-$NaYF_4$:Yb(20%),Tm(0.5%) NCs. Monodisperse β-$NaYF_4$:Yb,Tm NCs were prepared with a user-friendly protocol we previously developed.[30] All the chemical reagents were used as received without further purification. At the beginning, 0.8 mmol YCl_3, 0.2 mmol $YbCl_3$, 0.05 mmol $TmCl_3$ were mixed with 4 mL oleic acid and 16 mL octadecene (ODE) in a 50-mL three-neck flask. The solution was heated to 160 ˚C to form a yellow transparent solution and then cooled down to room-temperature. Subsequently, 10 mL of methanol solution containing 2.5 mmol NaOH and 4 mmol NH_4F was added into the flask and stirred for 30 min. After that, the solution was slowly heated to remove methanol and degassed at 100 ˚C for 20 min. The flask was heated to 300 ˚C and maintain at this temperature for 1.5 h under Ar protection. After naturally cooling down to room-temperature, the products were precipitated from the solution by ethanol and centrifuged out with a speed of 5 000 rpm. The products were washed with cyclohexane and ethanol for four times, and finally dispersed in cyclohexane with a concentration around 0.1 M.

2.2 Coating carbon shell on β-$NaYF_4$:Yb,Tm NCs. The above β-$NaYF_4$:Yb,Tm NCs were initially modified with surfactant to become hydrophilic and then used as seeds to coat a carbon shell using hydrothermal approach. In a typical synthesis, 10 mL deionized (DI) water and 0.05 g cetyltrimethyl ammonium bromide (CTAB) were mixed in a 25-mL flask and heated to 40 ˚C for 10 min for fast dissolution of the surfactant. Then, 0.02 mmol $NaYF_4$:Yb,Tm NCs in cyclohexane solution were added to above solution and the temperature was raised to 78 ˚C for slowly evaporating the cyclohexane. After a transparent solution was formed, the solution was transferred into a 50-mL autoclave. Following the addition of 0.4 g glucose inside, the autoclave

was heated to 160 °C and maintained at this temperature for 4 h. After the autoclave was cooled down to room-temperature, the products were centrifuged off from the solution and washed with ethanol and DI water, and finally dispersed in DI water for the next step.

2.3 Deposition of CdS nanoclusters on NaYF$_4$:Yb,Tm@C NPs. In a typical synthesis, 15 mL DI water and 0.02 mmol NaYF$_4$:Yb,Tm@C NPs were mixed in a 25-mL flask. The solution was heated to 80 °C, following the addition of 0.5 g polyvinylpyrrolidone (PVP) and 0.026 g Cd(NO$_3$)$_2$·4H$_2$O inside. The solution was then kept under stirring for 30 min for the adsorption of Cd^{2+} ions on the carbonous shell of NaYF$_4$:Yb,Tm@C NPs. Subsequently, 0.026 g thioacetamide (TAA) were added to the solution and the solution was stirred at 80 °C for 1 h. The flask was then equipped with a condenser and put in the microwave irradiator (MCR-3E, 280W) and irradiated for 10 min. After the microwave irradiator was turned off, the products were centrifuged off from the flask and washed with DI water and ethanol thrice. Finally, the products were dried in vacuum at 60 °C for 4 h.

2.4 Characterizations. Powder X-ray diffraction (XRD) was carried out on a Philips X'Pert Pro X-ray diffractometer equipped with Cu Kα radiation. Transmission electron microscopy (TEM) and energy dispersive X-ray spectroscopy (EDS) were performed on a JEOL 2010F TEM operated at 300 kV. The TEM samples were prepared by dropping a suspension of NPs on a copper grid. Scanning electron microscopy (SEM) was obtained with a Hitachi S-4800 field emission SEM with an accelerating voltage of 15 kV. Fluorescence spectra were acquired on a Hitachi F-7000 spectrometer equipped with a commercial 980-nm NIR laser. UV-Vis absorption spectra were obtained on a Shimazhu UV-2450 UV-Vis spectrometer. X-ray photoelectron spectroscopy (XPS) measurements were done on a ESCALAB MKII XPS system with Mg Kα source and a charge neutralizer.

2.5 Photocatalytic measurements. Photocatalytic activities of the β-NaYF$_4$:Yb,Tm@C@CdS NPs were evaluated by degradation of rhodamine B (RhB) and methylene blue (MB) solutions under the irradiation of a Xe lamp (50W), respectively. Different irradiation bands were obtained through rationally choosing the following filters: Vis bandpass (400-780 nm) and NIR bandpass (780-2500 nm). In a typical process, 10 mg of the as-prepared products was put into 50 mL RhB solution or MB solution (5×10^{-5} M) in a beaker. The solution was then stirred for 12 h in dark to reach an adsorption-desorption equilibrium between the NPs and the dye molecules.

Subsequently, the beaker was exposed to the irradiation of the Xe lamp accompanied with suitable filters. Aliquots were intermittently collected at given time intervals to measure the concentration of RhB or MB by UV-Vis spectroscopy.

3. Results and discussion

3.1 Synthetic strategy and formation mechanism. The synthetic process from primitive NaYF$_4$:Yb,Tm NCs to double shell-coated NaYF$_4$:Yb,Tm@C@CdS NPs is illustrated in Scheme 1. Since the prepared NaYF$_4$:Yb,Tm NCs have a hydrophobic surface due to the surface-adsorbed oleic acid (OA), they are unable to be dispersed in water. However, the process of hydrothermal carbonization of glucose is generally performed in aqueous solution. To modify the particles' surface, we employed a reverse micelle method to attach a monolayer of surfactants on these NCs (see Figure S1). The hydrophobic tails of surfactants can bind oleic acids on the NCs' surface through van der Waals interaction, leaving their hydrophilic heads pointing outward. After modification with surfactant, the NaYF$_4$:Yb,Tm NCs can be well dispersed in water and mixed with glucose solution. When the mixed solution was hydrothermally treated in an autoclave for 4 h, a layer of carbonous polymer is created on each NaYF$_4$:Yb,Tm particle. Note that the carbonous polymer shell consists of crosslinked aromatic compounds and lots of functional groups such as –OH, –CHO, and –COOH.[31] As such, the carbon shell can efficiently adsorb Cd^{2+} ions around the NaYF$_4$:Yb,Tm NCs. For deposition of small CdS NCs on these particles, we employ thioacetamide (TAA) as the sulfur source for it can slowly release S^{2-} ions into the solution upon heating. When plenty of Cd^{2+} ions are adsorbed in the carbon shell, the nucleation of CdS NCs will initiate within or around the shell. Owing to the confinement of the polymer shell, fast growth of CdS nuclei into big NCs is restrained and small CdS NCs are thus *in situ* produced around the particle. These tiny CdS NCs have a tendency to aggregate together in order to reduce their surface energy. As a result, formation of small nanoclusters is preferred under this system. At the same time, since the functional groups of the polymer shell can bind CdS nanoclusters through coordination, the produced CdS nanoclusters are covalently attached on the particle surface after deposition. However, it should be noted that CdS nanoclusters produced under this condition has a relatively poor crystallinity (stirring at 80 °C for 1 h). To enhance their crystallinities, we employed microwave irradiation as a post-treatment procedure because this method is rapid, convenient and low cost. In particular, this

method does not affect the morphology and structure of the samples since it happens in a very short of period and at relatively low temperature (80 ˚C for 10 min). After the microwave irradiation, crystalline CdS nanoclusters can be attained on the carbon shell-modified NaYF$_4$:Yb,Tm NCs.

TEM images of samples at different preparation stages verify the above proposed synthetic strategy (see Fig. 1). Fig. 1A is a typical TEM image of the prepared NaYF$_4$:Yb,Tm NCs. These NCs exhibit a hexagonal plate-like shape with a diameter of 200 nm (diagonal length) and thickness of *ca.* 160 nm. These NCs are uniform in sizes and apt to self-assemble on the copper grid due to the use of oleic acid (OA) as ligands during preparation. When these NaYF$_4$:Yb,Tm NCs were modified with surfactant and hydrothermally treated in the glucose solution, obvious shells were produced on their surface, implying the formation of carbon shells on each NaYF$_4$:Yb,Tm@C NC (see Fig. 1B). The carbon shell is around 30 nm in thickness. No free carbon sphere was produced as byproduct in our case when the concentration of glucose was diluted to some extent (~ 40 mg/mL). After the formation of a carbon shell, these core-shell NPs can be well dispersed in water for chemical adsorption of Cd^{2+} ions in aqueous solution. The adsorption of metal ions can be verified by the ICP measurement and this adsorption does not affect the morphology of the prepared NaYF$_4$:Yb,Tm@C NPs (see Fig. 1C). When the Cd^{2+}-saturated particles were mixed with TAA solution and treated under microwave irradiation, lots of CdS nanoclusters appeared on the NaYF$_4$:Yb,Tm@C NPs, suggesting the success of the designed strategy. The formation of CdS nanoclusters instead of a compact CdS shell may provide some unique advantages. Firstly, this morphology allows more NIR light to reach the core NaYF$_4$:Yb,Tm NCs due to the less scattering effect of the shell. Secondly, the reactant for catalysis can also be easily adsorbed by the carbon shell without any shielding effect from the shell. Sufficient adsorption of reactants is a crucial step for the whole photocatalytic process and it is also a key parameter to determine the overall efficiency of the photocatalysts.

3.2 SEM and TEM images. The morphologies of the prepared samples were characterized by both SEM and TEM (see Fig. 2). Fig. 2A displays a low-magnification SEM image of the NaYF$_4$:Yb,Tm@C@CdS NPs. From this image, one can see that these particles are uniform in size and can be prepared at large scale, showing good productivity of this method. The average diameter of the particles is about 250 nm. At higher magnification, it is observed that these particles are some big

spheres on which many small particles are attached (see Fig. 2B). TEM images of these particles give a better insight into their structural information. As shown in Fig. 2C, one can observe obvious core-shell structure on each particle according to the contrast between different components in a single particle. The black cores are the $NaYF_4$:Yb,Tm NCs with a diameter of 200 nm, and the gray shells of 30 nm are constituted by the crosslinked carbonous polymer. The black spots around the core-shell particles should be CdS nanoclusters. These small particles are around 10~30 nm in diameter. Under high-resolution TEM (see Fig. 2D), it is clearly observed that each CdS particle is not a single NC but consisting of a cluster of tiny CdS NCs (also see Fig. S2). One single cluster may contain 10~30 tiny NCs which is about 3~6 nm in size. Clear lattice fringes can be observed on each tiny NC in the clusters, showing its high crystallinity after microwave irradiation. The spacing between two fringes is 0.29 nm, matching well with the (200) plane of cubic CdS crystal. The orientation of these nanoclusters is not along the same direction, suggesting that these tiny NCs are randomly aggregate together, rather than following an oriented growth mechanism. The stability of the CdS nanoclusters on the carbon shell was also tested by repeating the ultrasonic treatment, washing and collection process. No obvious decrease in the number of CdS nanoclusters on each particle was found, suggesting that the carbon shell can firmly attach these nanoclusters due to the *in situ* deposition route and sufficient binding groups on the carbon shell.

3.3 Phases and compositions of samples. Fig. 3A gives the XRD pattern of the $NaYF_4$:Yb,Tm@C NPs before CdS coating. All the peaks are readily indexed to the pure hexagonal-phase $NaYF_4$ crystal (JCPDS stand card No. 16-0334). No peak from cubic-phase $NaYF_4$ crystal was found, showing high purity of the doped $NaYF_4$:Yb,Tm NCs. Note that there is also no peak from graphitized carbon was observed in the XRD patterns, suggesting that the shell is mainly constituted by carbonous polymer rather than graphitized carbon species. The polymeric feature is important for the shell to sufficiently absorb Cd^{2+} ions around the $NaYF_4$:Yb,Tm NCs. When the CdS nanoclusters were formed on the $NaYF_4$:Yb,Tm@C NPs, two sets of diffraction peaks can be observed (see Fig. 3B). One set of peaks match well with the hexagonal-phase $NaYF_4$ crystal while the other set of peaks are consistent with cubic CdS crystal (standard JCPDS card No. 89-0440). Evidently, this result suggests that the purity and crystallinity of $NaYF_4$:Yb,Tm cores were reserved during the post synthesis and the newly created CdS nanoclusters were pure in phase. EDS analyses

of the NaYF$_4$:Yb,Tm@C@CdS NPs are shown in Fig. S3 and Table S1 (supporting information). The existence of elements such as Na, F, Y, Yb, C, S and Cd, confirms the compositions of the NaYF$_4$:Yb,Tm@C@CdS NPs. The signal from Cu element and high intensity of C element in the EDS data is resulted from the carbon-film coated copper grid.

Fig. 4 shows the high-resolution XPS spectra of the NaYF$_4$:Yb,Tm@C@CdS NPs in which the elements Cd, S, Y, Na, Tm, and Yb are list, respectively. The C1s (284.1 eV) peak was used as an internal reference in the spectra. In Fig. 4A, the peaks of binding energies at 405.1 eV and 411.7 eV are attributed to core levels of Cd^{3+} 3d$_{5/2}$ and Cd^{3+} 3d$_{3/2}$, respectively. Two peaks located at 161.6 eV and 163.6 eV in Fig. 4B can be assigned to the core levels of S^{2-} 2p$_{1/2}$ and S^{2-} 2p$_{3/2}$. These results are in agreement with the reported core levels of CdS crystal, implying that these nanoclusters are pure CdS NCs. [32-33] Two XPS peaks at 161.2 eV and 159.3 eV are from Y^{3+} ions, corresponding to the Y^{3+} 3d$_{3/2}$ and Y^{3+} 3d$_{5/2}$, respectively (see Fig. 4C). The element Na displays one characteristic peak at 1071.4 eV due to the core level of Na 1s (see Fig. 4D). In addition to the main elements in the NaYF$_4$ NCs, the doping elements in these NCs can also been detected. The peaks at 171.9 eV, 174.2 eV (see Fig. 4E) and 182.3 eV (see Fig. 4F) are attributed to the Tm^{3+} ions and Yb^{3+} ions, respectively. The atomic ratios of these elements in the NaYF$_4$:Yb,Tm@C@CdS NPs have been list in the Table S2 (supporting information), which is close to the stoichiometric data of the sample.

3.3 Upconversion emissions and UV-Vis absorption. NaYF$_4$ NC is a typical nanoscale host-matrix for UC luminescence when doped with lanthanide ions.[34-35] When Yb^{3+} and Tm^{3+} are co-doped inside, the NaYF$_4$ NCs can give strong UC emissions upon NIR excitation in which the Yb^{3+} serves as sensitizer ions for continuous absorbing NIR light and the Tm^{3+} functions as activator ions to give various emissions. Fig. 5 displays the UC spectra of NaYF$_4$:Yb,Tm NCs under the excitation of 980-nm wavelength. One can see that four UC peaks, namely two UV emissions and two blue emissions, can be observed in the spectra. The UV emissions centered at 349 nm and 362 nm are attributed to the ^{1}I$_6$→^{3}F$_4$ and ^{1}D$_2$→^{3}H$_6$ transitions of Tm^{3+} ions while two blue emissions located at 450 nm and 476 nm can be assigned to the ^{1}D$_2$→^{3}F$_4$ and ^{1}G$_4$→^{3}H$_6$ of Tm^{3+} ions, respectively.[29,36] After modified with a carbon shell, the UC emissions of NaYF$_4$:Yb,Tm NCs slightly decreased due to the light absorption and scattering effect of the carbon shell (see Fig. 6). When the CdS

nanoclusters were deposited on the NaYF$_4$:Yb,Tm@C NPs, strikingly, all the four UC peaks dramatically reduced. Compared with the coated carbon shell, the CdS nanoclusters are less compact and do not have strong scattering effect to the incident NIR light. Therefore, the remarkable decrease in UC emissions should be attributed to the absorption of CdS nanoclusters. This result suggests that the UC emissions of core NaYF$_4$:Yb,Tm NCs upon NIR excitation can be effectively absorbed by the CdS nanoclusters on the shell.

UV-Vis absorption spectra of the NaYF$_4$:Yb,Tm NCs before and after carbon modification are shown in Fig. 6. Before coating, pure NaYF$_4$:Yb,Tm NCs does not have obvious absorption in the Vis region. However, a low and wide absorption appears from the carbon-shell coated NaYF$_4$:Yb,Tm NCs. This result is attributed to the absorbance of crosslinked carbonous polymer in the shell because they are constituted by many aromatic compounds. When CdS nanoclusters were deposited, the NaYF$_4$:Yb,Tm@C@CdS NPs exhibit a strong absorption in the Vis band. This absorption is similar to the absorption spectrum of pure CdS NCs which were prepared under microwave irradiation without the addition of NaYF$_4$:Yb,Tm@C seeds (see Fig. S4). The bandgap of these pure CdS NCs is calculated to be 2.55 eV, showing the effect of quantum confinement compared to bulk CdS (2.4 eV).[33] Comparing the UC spectra of NaYF$_4$:Yb,Tm NCs with the absorption spectra of CdS nanoclusters, one can easily recognize that all the four UC emissions of NaYF$_4$:Yb,Tm NCs can be readily absorbed by the surface CdS NCs. This implies that a high utilization efficiency of the NIR light may achieve through combining the NaYF$_4$:Yb,Tm UCNs and CdS nanoclusters together.

3.4   Photocatalytic   properties.   Photocatalytic   activity   of   the NaYF$_4$:Yb,Tm@C@CdS NPs was assessed by the degradation of two model pollutants (RhB and MB), respectively. Through monitoring the characteristic absorption of RhB (553 nm) and MB (664 nm) at given intervals, the activity of sample can be evaluated by UV-Vis spectrometer. Fig. 7A is the UV-Vis absorption spectra of RhB solution with a small amount of NaYF$_4$:Yb,Tm@C@CdS NPs (50 mg) under the Vis irradiation (400-780 nm). The concentration of RhB solution decreases very fast under the shinning of the Vis light, showing good catalytic activity of the sample. Considering that both NaYF$_4$:Yb,Tm NCs and the carbon shells have no catalytic effect under the Vis light (see Fig. 7B), such Vis-driven activity should be ascribed to the CdS nanoclusters on the hybrid NPs. Interestingly, when the same

photocatalytic experiments were carried out under the Vis-NIR band (400-2500 nm), a faster decrease in RhB concentration was observed (Fig. S5). Plotting the relative concentration C/C_0 *versus* the degradation time, the difference in the activity of sample under different irradiation bands can be observed (see Fig. 7B). Obviously, the $NaYF_4$:Yb,Tm@C@CdS NPs show an enhanced photocatalytic activity under the Vis-NIR band compared to that under pure Vis band. This result suggests that $NaYF_4$:Yb,Tm NCs can improve the activity of CdS nanoclusters by utilizing the NIR light. To confirm this hypothesis, we also carried out the same experiment under a NIR laser and obvious decrease in RhB concentration was also observed (see Fig. S6).

Although the carbon shell does not directly participate in the catalytic reaction, it has a strong adsorption to the dye molecules. In Fig. 7B, it was observed that the concentration of dyes has a notable decrease prior to light irradiation. Nearly fifteen percent of dyes have been absorbed by the catalysts regardless what kind of irradiation bands will be applied. Considering that both $NaYF_4$:Yb,Tm NCs and CdS nanoclusters just have slight adsorption to the dye molecules, such high adsorption capacity should be ascribed to the carbon shells. This is an important feature for the catalysts to improve their total catalytic activity. We also synthesized pure CdS NCs without the $NaYF_4$:Yb,Tm@C templates under the microwave irradiation (see Fig. S4). Under the Vis light, this sample indeed shows low adsorption to dye molecules and lower activity than the $NaYF_4$:Yb,Tm@C@CdS NPs (based on the same amount of CdS). This result further confirms that the carbon shell has a synergetic effect for the high activity of CdS nanoclusters.

The photocatalytic activity of the $NaYF_4$:Yb,Tm@C@CdS NPs was also evaluated with other dyes such as MB molecules (see Fig. 7C and 7D). Enhanced activity under the Vis-NIR band and strong adsorption to dye molecules by the carbon shells can both be observed. These results confirm the indispensable roles of the $NaYF_4$:Yb,Tm NCs and carbon shells in the hybrid catalysts. Apparent rate constants of the degradation experiments were also employed to show the catalytic efficiency of samples under different irradiation bands. As shown in Fig. S7 and Table S3 and S4, the catalytic efficiency of $NaYF_4$:Yb,Tm@C@CdS NPs under Vis-NIR band is higher than they working under the Vis band and pure CdS NCs under Vis band. These results further confirm the important function of UC cores and the carbon layer.

Photocatalytic activity of the mixture of $NaYF_4$:Yb,Tm and CdS (similar amounts as those in $NaYF_4$:Yb,Tm@C@CdS) was also assessed by the degradation of Rh.B

solution (see Fig. S8). The activity of this mixture is obviously lower than that of the NaYF$_4$:Yb,Tm@C@CdS NPs under different irradiation bands, particularly under the NIR band, implying that that the synthesis of uniform core-shell nanostructures with a carbon layer is crucial to their good photocatalytic properties. On the other hand, we have also attempted the synthesis of NaYF$_4$:Yb,Tm@C NPs with different carbon thickness (see Fig. S9). The result suggested thicker carbon shell would reduce the UC emissions of samples due to the absorption and light scattering effect. But pretty thin shell would lower the adsorption to dye molecules for subsequent catalytic applications (see Fig. S10). As such, a moderate carbon shell (i.e., 30 nm) between the NaYF$_4$:Yb,Tm and CdS nanoclusters is thus preferred for the consideration of both energy transfer and dye adsorption.

3.5 Working mechanism of the hybrid photocatalysts. It is well established that photocatalytic oxidation of organic pollutants is initiated by the reactive species such as photogenerated holes (h$^+$), hydroxyl radicals (•OH) and superoxide radicals (•O$_2^-$). In our experiments, the active species generated from the NaYF$_4$:Yb,Tm@C@CdS NPs were also investigated under the NIR light. Three kinds of scavengers (i.e., ammonium oxalate (AO), tertiary butanol (t-BuOH) and benzoquinone (BQ)), were separately introduced to the degradation process of RhB molecules for trapping the h$^+$, •OH and •O$_2^-$, respectively. As shown in Fig. 8, the degradation rate is significantly restrained in the presence of BQ (•O$_2^-$ scavenger), inferring that •O$_2^-$ should be a major contributor to the decomposition of the dye molecules. When AO was introduced to the system to suppress the photogenerated h$^+$, the degradation rate is also greatly reduced, revealing that h$^+$ is also a main reactive species to the photocatalytic oxidation process. However, if t-BuOH was added as a scavenger of •OH, the degradation rate only showed a slight decrease, suggesting that •OH is not a dominant active species. This result may attribute to the fact that the valence band (VB) edge of CdS (~1.65 V *vs.* NHE, pH=7) is less positive than the standard potential of •OH/OH$^-$ (~2.38 V *vs.* NHE, pH=7).[37-38] As such, the photogenerated h$^+$ cannot efficiently oxidize OH$^-$ groups to be •OH radicals. The existence of very few •OH radicals in the system may be evolved from the •O$_2^-$ radicals. We also conducted above three scavenger experiments under Vis light and found that the results were much similar to those under the NIR light. This result confirms that CdS nanoclusters are the catalytic part for generating reactive species in the hybrid photocatalysts and the NaYF$_4$:Yb,Tm NPs serve as light transducers.

Based on the UC spectra and the detected reactive species, the enhanced mechanism of the hybrid $NaYF_4$:Yb,Tm@C@CdS photocatalysts under NIR light can be illustrated in Scheme 2. Firstly, the Yb^{3+} ions serve as sensitizer ions to absorb the NIR light in the Yb^{3+} and Tm^{3+} co-doped $NaYF_4$ NCs. When the excited Yb^{3+} ions relax from $^2F_{5/2}$ level to $^2F_{5/2}$ level, they will successively transfer energy to the near Tm^{3+} ions. Through a typical energy transfer upconversion (ETU) process, the Tm^{3+} ion are excited to the $^3H_5$ level and then relax nonradiatively to the $^3F_4$ level. Successive ET from Yb^{3+} to Tm^{3+} leads to the population of the $^3F_2$ level of Tm^{3+}.[21] Afterwards, the $^3F_2$ level relaxes to the $^3H_4$ level and then is excited to the $^1G_4$ level by ET from other excited Yb^{3+} ions.[39] Because of the large energy mismatch (about 3500 cm^{-1}), the $^1G_4$ level cannot be directly populated to the $^1D_2$ level by the fourth photon from Yb^{3+} *via* ET process. The population of $^1D_2$ level may be realized by two cross relaxation processes: $^3F_2 + {}^3H_4 \rightarrow {}^3H_6 + {}^1D_2$ and $^1G_4 + {}^3H_4 \rightarrow {}^3F_4 + {}^1D_2$.[40] After that, the excited Tm^{3+} ions fall to lower energy levels: $^1I_6 \rightarrow {}^3F_4$, $^1D_2 \rightarrow {}^3F_4$, $^1G_4 \rightarrow {}^3H_6$, $^1D_2 \rightarrow {}^3H_6$, and $^1G_4 \rightarrow {}^3F_4$, leading to the emission of 345 nm, 368 nm, 450 nm, and 475 nm, respectively.[39,40] The energy gap of CdS is about 2.4 eV, and hence all the four UC emissions from $NaYF_4$:Yb,Tm NCs can be absorbed by CdS nanoclusters. Under the excitation of these UC emissions, the activated CdS nanoclusters produce photoelectrons (e^-) and holes (h^+) in the CB and VB bands, respectively, and then migrate from the inner region to the surface. When reaching the dye molecules, the h^+ can directly function as an oxidant while the e^- will reaction with O_2 and produce $\cdot O_2^-$ species. Both of the h^+ and $\cdot O_2^-$ can be directly utilized for the photocatalytic oxidation of dye molecules. Though the carbon layer does not directly participate in the reaction, it also plays two important roles: 1) serving as an adsorber to enrich the dye molecules around the photocatalysts; 2) working as a firm substrate to fix the CdS nanocluster around the carbon-coated $NaYF_4$:Yb,Tm NCs.

4. Conclusions

In summary, we have developed a facile strategy to construct hybrid NIR-activated photocatalysts with a uniform core-shell structure. High-quality hydrophobic $NaYF_4$:Yb,Tm were modified with a carbon layer through the reverse micelle method. The carbon layer-modified $NaYF_4$:Yb,Tm NCs not only become hydrophilic but also provide a good substrate for CdS deposition. The developed $NaYF_4$:Yb,Tm@C@CdS NPs can work under NIR light as photocatalysts through upconverting the NIR

photons to be UV and Vis ones. Due to the NIR utilization and the adsorption capability of the carbon layer, the developed photocatalysts exhibit good photocatalytic activity under the Vis light and obviously enhanced performance under the Vis-NIR light. The working mechanism of this hybrid NIR-activated photocatalyst has also been proposed.

Acknowledgements

References:

1. A. Kudo and Y. Miseki, *Chem. Soc. Rev.*, 2009, **38**, 253-278.

2. X. B. Chen, S. H. Shen, L. J. Guo and S. S. Mao, *Chem. Rev.*, 2010, **110**, 6503-6570.

3. H. Tong, S. X. Ouyang, Y. P. Bi, N. Umezawa, M. Oshikiri and J. H. Ye., *Adv. Mater.*, 2012, **24**, 229-251.

4. C. C. Chen, W. H. Ma and J. C. Zhao, *Chem. Soc. Rev.*, 2010, **39**, 4206-4219.

5. Q. J. Xiang, J. G. Yu and M. Jaroniec, *Chem. Soc. Rev.*, 2012, **41**, 782-796.

6. S. Bai, J. Jiang, Q. Zhang and Y. J. Xiong, *Chem. Soc. Rev.,* 2015, **44**, 2893-2939.

7. R. Asahi, T. Morikawa, T. Ohwaki, K. Aoki and Y. Taga, *Science*, 2001, **293**, 269-271.

8. P. Wang, J. Wang, T. S. Ming, X. F. Wang, H. G. Yu, J. G. Yu, Y. G. Wang and M. Lei, *ACS Appl. Mater. Inter.*, 2013, **5**, 2924-2929.

9. L. Li, S. Q. Zhou, E. J. Chen, R. Qiao, Y. J. Zhong, Y. Zhang and Z. Q. Li, *J. Mater. Chem. A*, 2015, **3**, 2234-2241.

10. W. J. Zhou, Z. Y. Yin, Y. P. Du, X, Huang, Z. Y. Zeng, Z. X. Fan, Hong Liu, J. Y. Wang and H. Zhang. *Small*, 2013, **9**, 140-147.

11. W. Zhao, W. H. Ma, C. C. Chen, J. C. Zhao and Z. G. Shuai, *J. Am. Chem. Soc.,* 2004, **126**, 4782-4783.

12. M. Liu, X.Q. Qiu, M. Miyauchi and K. Hashimoto, *J. Am. Chem. Soc.*, 2013, **135**, 10064-10072.

13. A. Kubacka, M. F. García and G. Colón, *Chem. Rev.*, 2012, **112**, 1555-1614.

14. Y. T. Dong, J. Choi, H. K. Jeong and D. H. Son, *J. Am. Chem. Soc.,* 2015, **137**, 5549-5554.

15. S. Q. Huang, N. W. Zhu, Z. Y. Lou, L. Gu, C. Miao, H. P. Yuan and A. D. Shan, *Nanoscale*, 2014, **6**, 1362-1368.

16. W. Wang, M. Y. Ding, C. H. Lu, Y. R. Ni, Z. Z. Xu, *Appl. Catal. B*, 2014, **144**, 379-385.

17. Y. W. Zhang and Z. L. Hong, *Nanoscale*, 2013, **5**, 8930-8933.

18. W. K. Su, M. M. Zheng, L. Li, K. Wang, R. Qiao, Y. J. Zhong, Y. Hu and Z. Q. Li,

J. Mater. Chem. A, 2014, **2**, 13486-13491.

19. Y. X. Guo, H. W. Huang, Y. He, N. Tian, T. R. Zhang, P. K. Chu, Q. An and Y. H. Zhang. *Nanoscale*., 2015, **7**. 11702-11711.

20. C. H. Li, F. W, J. Zhu and J. C. Yu, *Appl. Catal. B*, 2010, **100**, 433-439.

21. G. Y. Chen, H. L. Qiu, P. N. Prasad and X. Y. Chen, *Chem. Rev*., 2014, **114**, 5161-5214.

22. F. Wang and X. G. Liu, *Acc. Chem. Res*., 2014, **47**, 1378-1385.

23. Y. Hu, Y. Liu, H. S. Qian, Z. Q. Li and J. F. Chen, *Langmuir*, 2010, **26**, 18570-18575.

24. D. A. Bulushev, L. G. Bulusheva, S. Beloshapkin, T. O'Connor, A. V. Okotrub and K. M. Ryan, *ACS Appl. Mater. Inter*., 2015, **7**, 8719-8726.

25. M. J. Zhou, Y. Hu, Y. Liu, W. L. Yang and H. S. Qian, *CrystEngComm*, 2012, **14**, 7686-7693.

26. A. J. Romero-Anaya, M. Ouzzine, M. A. Lillo-Ro´denas and A. Linares-Solano, *Carbon*, 2014, **68**, 296-307.

27. Y. Hu, X. H. Gao, L.Yu, Y. R. Wang, J. Q. Ning, S. J. Xu and X. W. Lou, *Angew. Chem. Int. Ed*., 2013, **52**, 5636-5639.

28. P. Zabek, J. Eberl and H. Kisch, *Photochem, Photobiol. Sci*., 2009, **8**, 264-269.

29. S. Sato, *Langmuir*., 1988, **4**, 1156-1161.

30. Z. Q. Li, Y. Zhang and S. Jiang, *Adv. Mater*., 2008, **20**, 4765-4769.

31. Y. Zhao, W. Li, X. Zhao, D. P. Wang and S. X. Liu, *Mater. Res. Innov*., 2013, **17**, 546-551.

32. J. J. Li, Y. A. Wang, W. Z. Guo, J. C. Keay|, T. D. Mishima, M. B. Johnson and X. G. Peng, *J. Am. Chem. Soc.,* 2003, **125**, 12567-12575.

33. J. G. Yu, Y. F. Yu, P. Zhou, W. Xiao and B, Cheng, *Appl. Catal. B*, 2014, **156-157**, 184–191.

34. G. F. Wang, Q. Peng and Y. D. Li. *Acc. Chem. Res*., 2011, **44**, 322-332.

35. F. Wang and X. G. Liu. *J. Am. Chem. Soc.,* 2008, **130**, 5642-5643.

36. C. X. Li, Z. W. Quan, J. Yang, P. P. Yang and J. Lin. *Inorg. Chem*., 2007, **46**, 6329−6337.

37. T. Simon, N. Bouchonville, M. J. Berr, A. Vaneski, A. Adrovic, D. Volbers, R. Wyrwich, M. Doblinger, A. S. Susha, A. L. Roach, F. Jackel, J. K. Stolarczyk and J. Feldmann, *Nat. Mater.*, 2014, **13**, 1013-1018.

38. S. Pasternak and Y. Paz, *ChemPhysChem*, 2013, **14**, 2059-2070.

39. J. Zhou, Z. Liu and F. Y. Li, *Chem. Soc. Rev.*, 2012, **41**, 1323-1349.

40. Y. N. Tang, W. H. Di. X. S. Zhai, R. Y. Yang and W. P. Qin, *ACS Catal.*, 2013, **3**, 405-412.
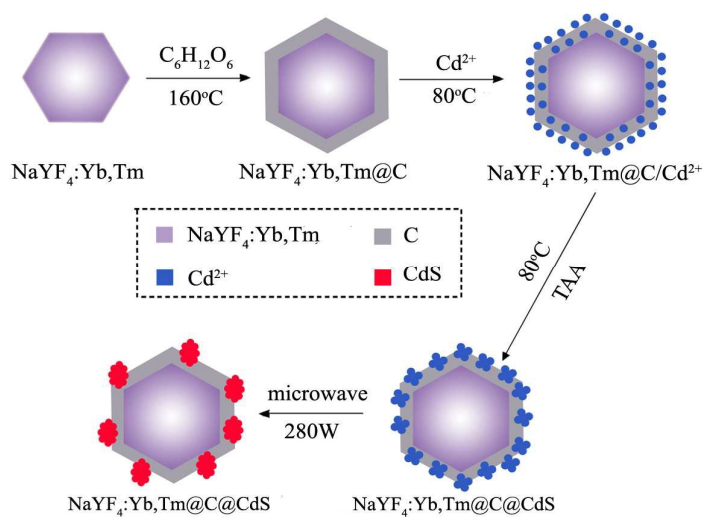
Scheme 1. Illustration of the synthetic strategy for preparing the core-shell NaYF$_4$:Yb,Tm@C@CdS NPs.
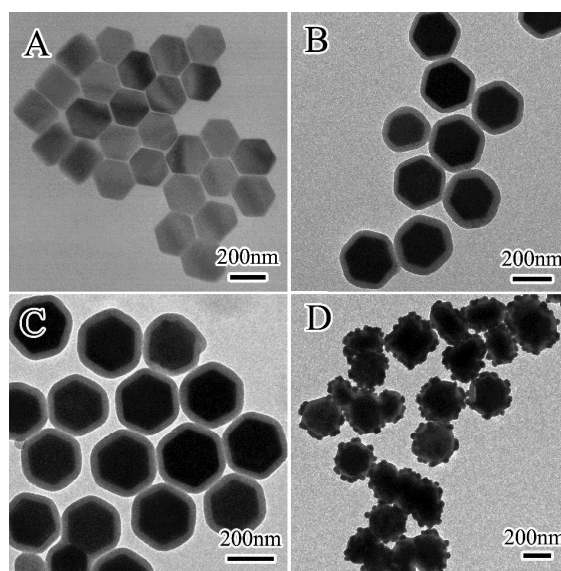
Figure 1. TEM images of samples obtained at different synthetic stages: (A) NaYF$_4$:Yb,Tm NCs; (B) carbon-coated NaYF$_4$:Yb,Tm NPs; (C) NaYF$_4$:Yb,Tm@C after Cd^{2+} adsorption; (D) NaYF$_4$:Yb,Tm@C@CdS NPs.
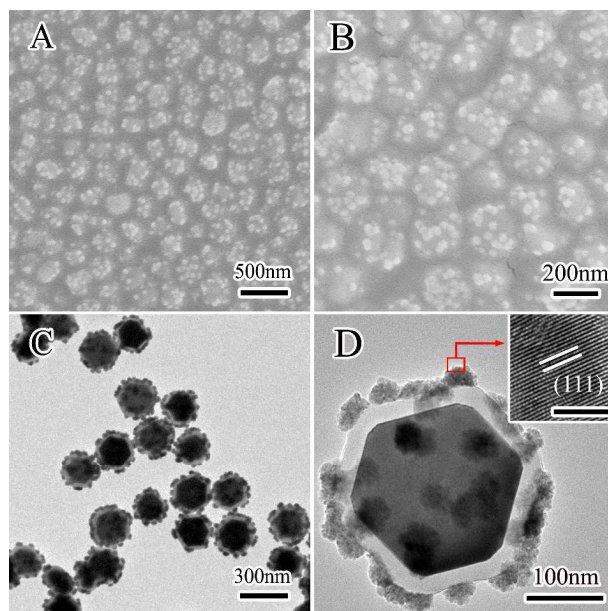
Figure 2. (A) and (B) are SEM images of the prepared NaYF$_4$:Yb,Tm@C@CdS NPs at different magnifications; (C) is the normal TEM image and (D) is the high-resolution TEM images of the products (scale bar in inset: 5 nm).
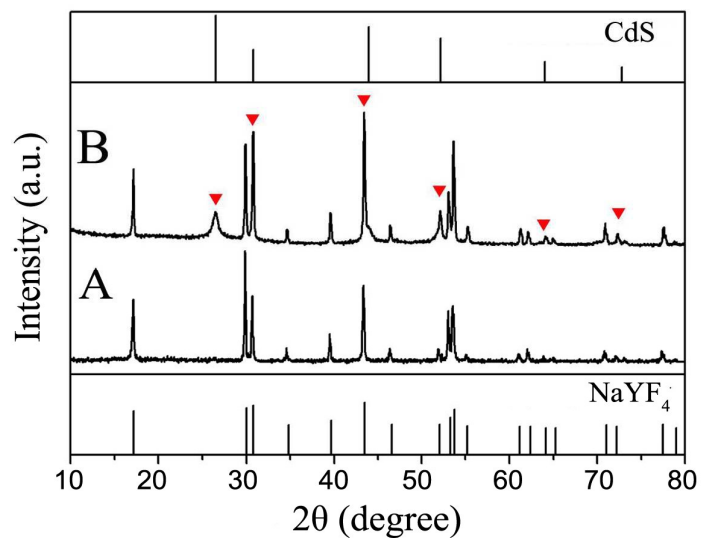
Figure 3. XRD patterns of the NaYF$_4$:Yb,Tm@C NPs (A) and the NaYF$_4$:Yb,Tm@C@CdS NPs (B). Standard XRD patterns of NaYF$_4$ and CdS crystal are also given as references.
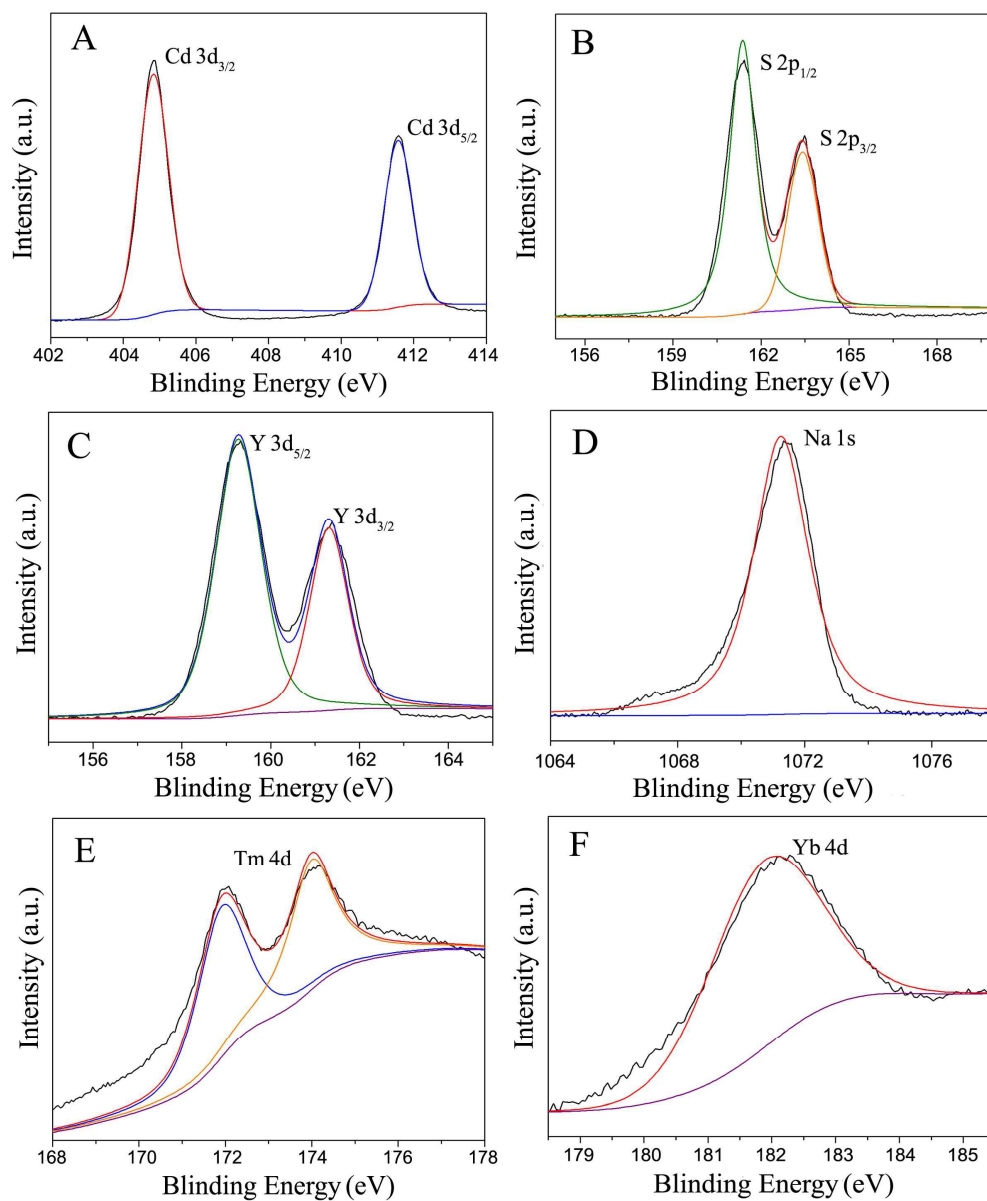
Figure 4. High-resolution XPS analyses of the NaYF$_4$:Yb,Tm@C@CdS NPs: (A) Cd 3d, (B) S 2p, (C) Y 3d, (D) Na 1s, (E) Tm 4d and (F) Yb 4d.
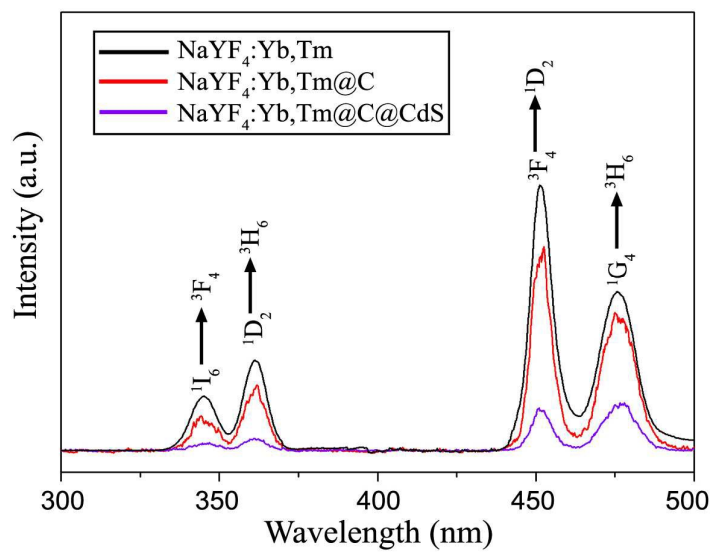
Figure 5. Upconversion PL spectra of the NaYF$_4$:Yb,Tm NCs (black), NaYF$_4$:Yb,Tm@C NPs (red) and NaYF$_4$:Yb,Tm@C@CdS NPs (purple) under 980 nm excitation.
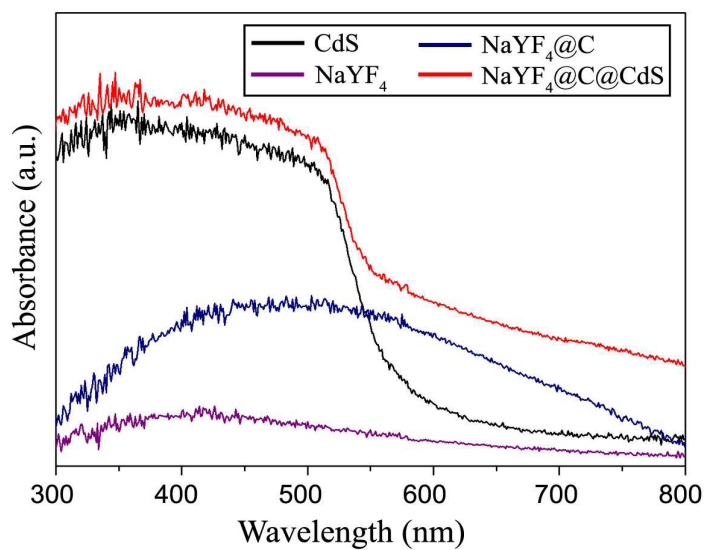
Figure 6. UV-Vis absorption spectra of the NaYF$_4$:Yb,Tm NCs (purple), pure CdS NCs (black), NaYF$_4$:Yb,Tm@C NPs (blue) and NaYF$_4$:Yb,Tm@C@CdS NPs (red).
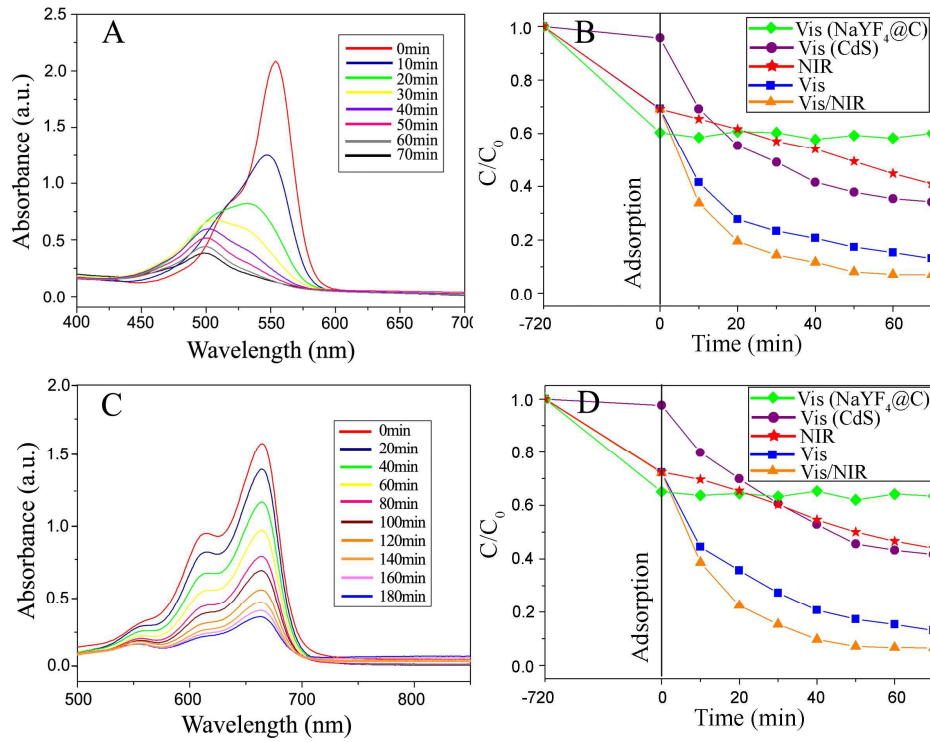
Figure 7. Photocatalytic activities of the NaYF$_4$:Yb,Tm@C@CdS NPs on the degradation of RhB and MB solutions. (A) and (C) are UV-Vis absorption spectra of RhB solution and MB solution under the catalysis of samples, respectively; (B) and (D) are comparisons of samples' activities under different irradiation bands.
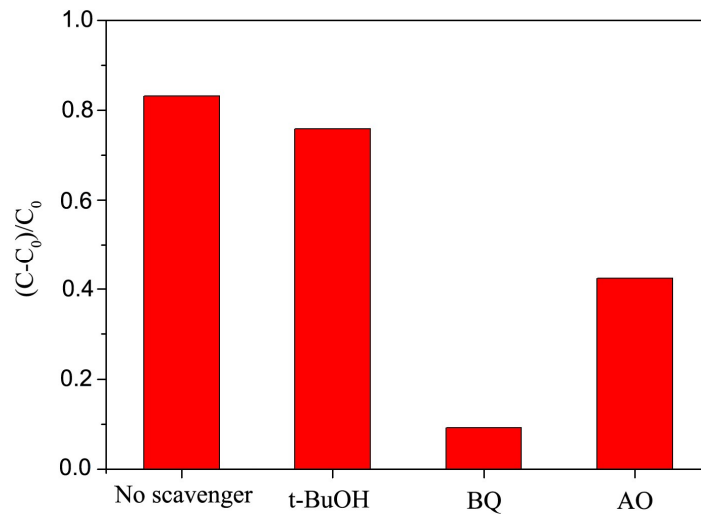
Figure 8. Photocatalytic activity of the $NaYF_4$:Yb,Tm @C@CdS NPs in the presence of different scavengers under NIR light on the degradation RhB solution.
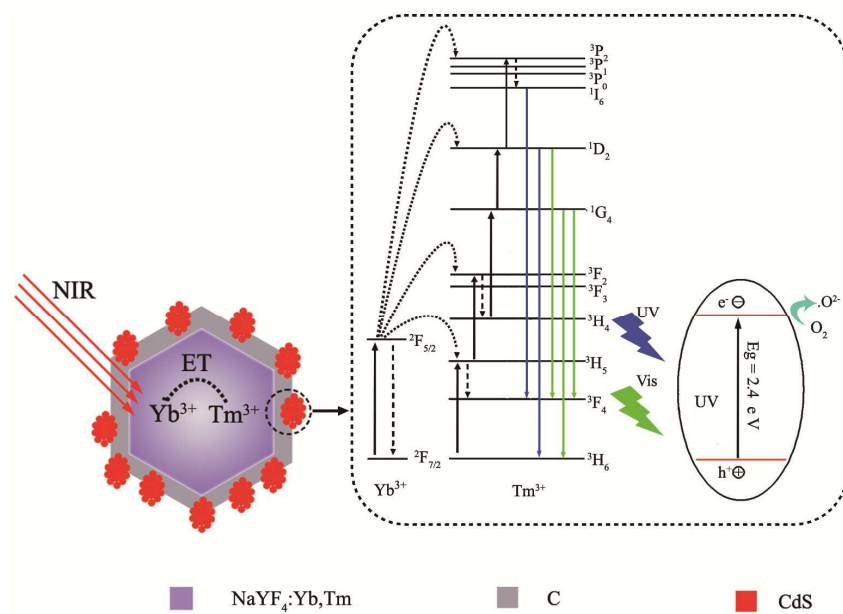
Scheme 2. Diagrams of the energy levels for the upconversion process and NIR light-driven photocatalytic mechanism of the $NaYF_4$:Yb,Tm@C@CdS NPs.